Master's Thesis of Engineering

Fabrication of high efficiency perovskite solar cells with anionic surfactants

음이온계 계면활성제를 활용한 고성능 페로브스카이트 태양전지의 제조

February 2021

Graduate School of Chemical and Biological Engineering

Seoul National University

Polymers and Organic Materials Major

Jeong Hun Lee

Fabrication of high efficiency perovskite solar cells with anionic surfactants

Advisor. Joon Hak Oh

Submitting a master's thesis of Engineering

February 2021

Graduate School of Chemical and Biological Engineering

Seoul National University

Polymers and Organic Materials Major

Jeong Hun Lee

Confirming the master's thesis written by
Jeong Hun Lee
February 2021

Chair	Jong-Chan Lee	(Seal)
Vice Chair	Joon Hak Oh	(Seal)
Examiner	Dongwon Yoo	(Seal)

Abstract

Controlling the crystal growth in the solution process is the most effective way to achieve high efficiency and high stability perovskite solar cells. However, the dynamic and rapid evaporation of the solvent makes it difficult to realize the high performance devices. In this study, an additive engineering using anionic surfactant was developed to boost the performance of perovskite solar cells. The efficiency and stability of perovskite solar cells were greatly increased by adding anionic surfactants to the lead halide-based perovskite. The anionic surfactants reduced the surface tension of the perovskite solution and increased the affinity with the substrate, enhancing the crystal growth of perovskite. Furthermore, the negative ions significantly improved the optical performance of lead-based perovskites by passivating uncoordinated lead defects. The perovskite solar cells with the anionic surfactants showed the reliable efficiency of 17.21%, exhibiting greatly reduced the hysteresis phenomenon which was commonly seen in perovskite solar cells. In addition, the addition of anionic surfactant increased the stability in both air and water. This method could be suggested as an effective way for commercialization of perovskite solar cells.

Keywords : Perovskite, Solar Cells, Additives, Anionic Surfactant, Passivation, Stability

Student Number : 2019-25885

Table of Contents

List of Figures and Tables

Chapter 1. Introduction

1.1. Perovskite Solar Cells

Solar cells have been widely studied in the next-generation renewable energy field. The inorganics, mostly silicon solar cells[1-4], showed superb efficiency with high stability, but they had expensive fabrication costs due to ultra-high purity of silicon required many processing steps. The organics, practically polymer[5-7] and small molecule[8-10] solar cells, had simple and low-cost processes, but their efficiency has stagnated below 16%, limiting their practical use.[11] The perovskites[12-15], containing both inorganic and organic materials, have been highlighted to overcome the problems (Figure 1.1).

Perovskites were generally classified into oxides[16,17] and halides[18,19] according to types of negative ions used for the anion site. The halide perovskites were commonly used as a solar cell material, based on better semiconducting properties than oxides. Perovskite's ABX_3 formula was first reported in 1978 with small cations, such as MA^+, FA^+, and Cs^+, as A, heavy metal cations, such as Pb^{2+} and Sn^{2+} as B, and halogen anions, such as Cl^-, Br^-, and I^-, as X (Figure 1.2a). In particular, tin-based perovskites have been drawn attention, because of the environmental pollution of lead-based perovskite.[20-23]

The perovskite was suggested as the active material for use in the solar cells, due to its high absorptions over the visible region, low exciton binding energy, large charge carrier diffusion lengths, and tunable band gap.[24-26] The superb optical and electrical properties of perovskite materials made the $MAPbI_3$-based perovskite solar cells could theoretically exhibit the efficiency of 30.6%, V_{oc} of 1.315 V, J_{sc} of 25.27 mA/cm^2, and FF of 0.91.[27]

The general structures of perovskite solar cells were presented (Figure 1.2b). Specifically, the perovskite solar cells consisted of planar junction with perovskites, n-type, and p-type

semiconductors unlike organic solar cells in which form a bulk-heterojunction. The photo-generated charge carriers in perovskite layer, especially electrons and holes, were selectively collected by the electron transport layer (ETL) and hole transport layer (HTL), respectively (Figure 1.2c). In this transport processes, the difference in fermi level between materials acted as charge injection barriers, which could greatly change the performance of perovskite solar cells.[28]

The first all-solid-state perovskite solar cells developed in 2009 showed a power conversion efficiency (PCE) of 8.51% by mimicking the architecture of dye-sensitized solar cells.[29] The efficiency of 23.32% was reported by the Chinese Academy of Sciences in 2019 (Figure 1.2d).[30] Very recently, the highest efficiency, reported by KRICT/MIT, was 25.2%.[31]

The general characteristics of the perovskite solar cells, such as the current density-voltage ($J-V$) curves, were similar to conventional silicon solar cells, indicating that their general analysis could be applied.[32] In general, the performance of solar cells could be described by several parameters. J_{sc} was the current density in the short circuit condition (Maximum current in the solar cell operation), and V_{oc} was the voltage in the open circuit condition (Maximum voltage in the solar cell operation). FF was the fill factor determined by the following formula,

$$FF = \frac{Real\ solar\ cell\ power\ (Maximum\ area\ of\ green\ box)}{Theoretical\ solar\ cell\ power\ (Area\ of\ red\ box)}$$

$$FF = \frac{Real\ solar\ cell\ power\ (Maximum\ area\ of\ green\ box)}{J_{sc} \times V_{oc}}$$

and PCE was obtained by dividing the solar cell power by the solar power (Figure 1.3a).

$$PCE = \frac{Real\ solar\ cell\ power\ (Maximum\ area\ of\ green\ box)}{Solar\ power}$$

$$PCE = FF \times \frac{J_{sc} \times V_{oc}}{Solar\ power}$$

In the case of the perovskite solar cells, the hysteresis phenomenon could occur due to the characteristics of the ion-bonding materials.[33,34] As a results, different efficiencies were exhibited depending on the scan directions. In order to compare the performances, the hysteresis index (HI) was introduced as quantitative factor, which was determined by the following formula (Figure 1.3b).[35]

$$HI = \frac{Reverse\ \ scan\ \ power - Forward\ \ scan\ \ power}{Reverse\ \ scan\ \ power}$$

1.2. Surfactants

Perovskite solar cells have been widely fabricated by spin-coating method.[36-40] The dynamic and rapid evaporation of solvent causes several problems in perovskite growth, such as pin hole defects formation, irregular grain growth, contact issues with ETL and HTL, and low purity of perovskite films. The researchers studied an anti-solvent,[41,42] interface modification,[43,44] and additive[45,46] methods to control perovskite growth. The surfactant additive methods have recently been studied as a novel method for fabricating uniform and highly reproducible perovskite solar cells with high efficiency.[47,48]

Surfactants typically consisted of a hydrophilic head and a hydrophobic tail with neutral, anionic, and cationic head, and the generally alkyl chain tail (Figure 1.4a). The surfactants were existed in various phases depending on their concentrations in solutions. Especially at the high concentration, micelle structures were formed, which could be apply to various polymerization methods[49,50] and drug delivery systems.[51,52] In the case of low concentrations, the surfactants were located on the surface of the solution, playing critical roles during spin-coating steps. The surfactants were added to the charge transport layer[53] or the active layer[54], facilitating

solution wetting and improving performances. In detail, the surfactant was located on the surface of the perovskite solution, enabling uniform perovskite crystal growth by reducing the surface tension (Figure 1.4b), and increasing the affinity between the hydrophobic surface and the solution, enabling dense crystal growth (Figure 1.4c).[47] In addition, some heads allowed hydrophobic surfactants to be located on the perovskite film surface and grain boundaries through the interaction with perovskite crystals. The surfactants could also act as molecular barriers for the diffusion of H_2O and O_2, extending the lifetime of perovskite solar cells (Figure 2. d).[48]

1.3. Background of Research

As mentioned above, the perovskite solar cells could overcome the shortcomings of conventional inorganic and organic solar cells by synergistically combining the advantages of each component, leading to the fabrication of high PCE solar cells prepared at a low processing cost. However, the low atmosphere stability of perovskite and the non-uniform perovskite crystal growth during spin coating process still remained challenging issues. Using surfactant additives might solve these problems. A small amount of surfactant could reduce the surface tension of the solution and increase the affinity with the hydrophobic substrate.

In this work, we searched for surfactants that could be solution processable, then applied them to the fabrication of perovskite solar cells. For this purpose, potassium perfluorobutane sulfonate (PFC) was developed. The formation of high purity perovskite film was confirmed through XRD analysis, and the passivation effect of sulfonate(anion) was confirmed through XPS analysis. In addition, the characteristics of the perovskite film were analyzed using SEM and AFM analyses. Their charge transport was studied using photoluminescence (PL) and time-resolved photoluminescence (TRPL) analyses, and the characteristics of the fabricated perovskite solar cells were investigated by measuring the $J-V$ properties. Finally, the stability tests of perovskite solar cells were conducted.

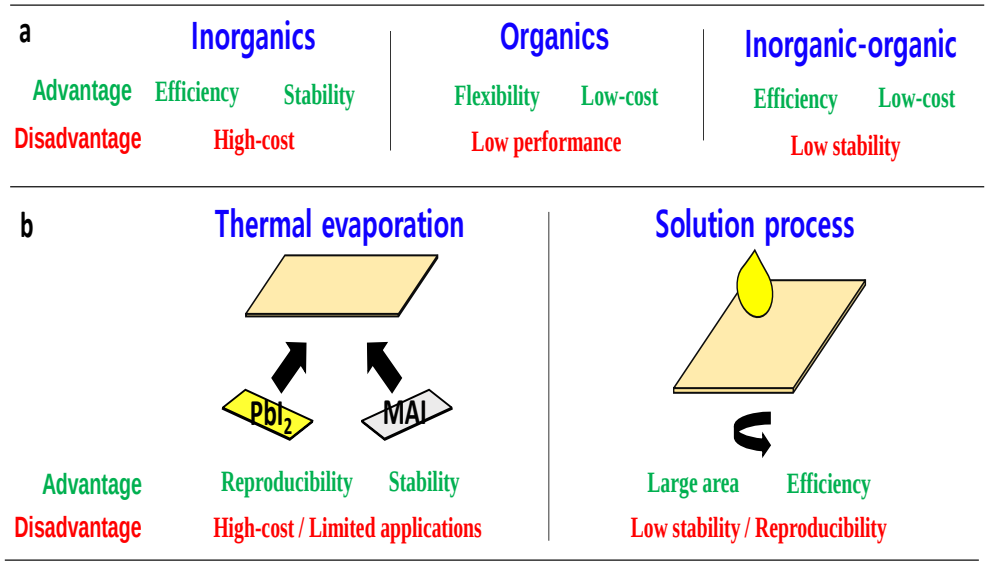

Figure 1.1. a. Summary of three different solar cells. b. Summary of two different fabrication processes.

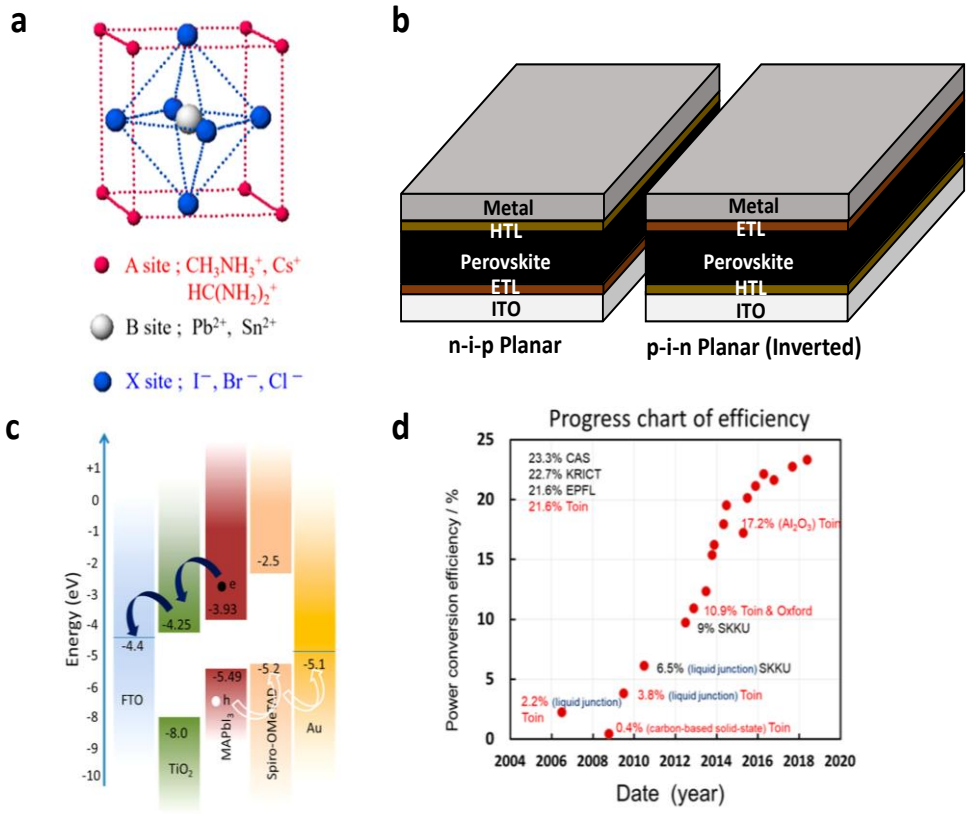

Figure 1.2. a. Structure of inorganic–organic metal halide perovskite crystal. b. Device structure of perovskite solar cells c. Energy diagram of conventional perovskite solar cells. d. Progress chart of power conversion efficiency.[55]

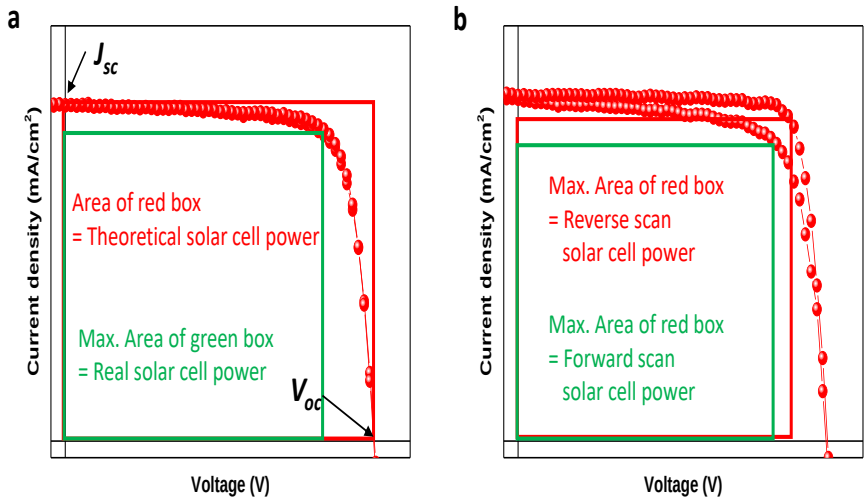

Figure 1.3. Schematic image of solar cell operations. a. The current density−voltage ($J-V$) curve of general solar cells. b. The current density−voltage ($J-V$) curve of some perovskite solar cells. The performance parameters are marked on the $J-V$ curve.

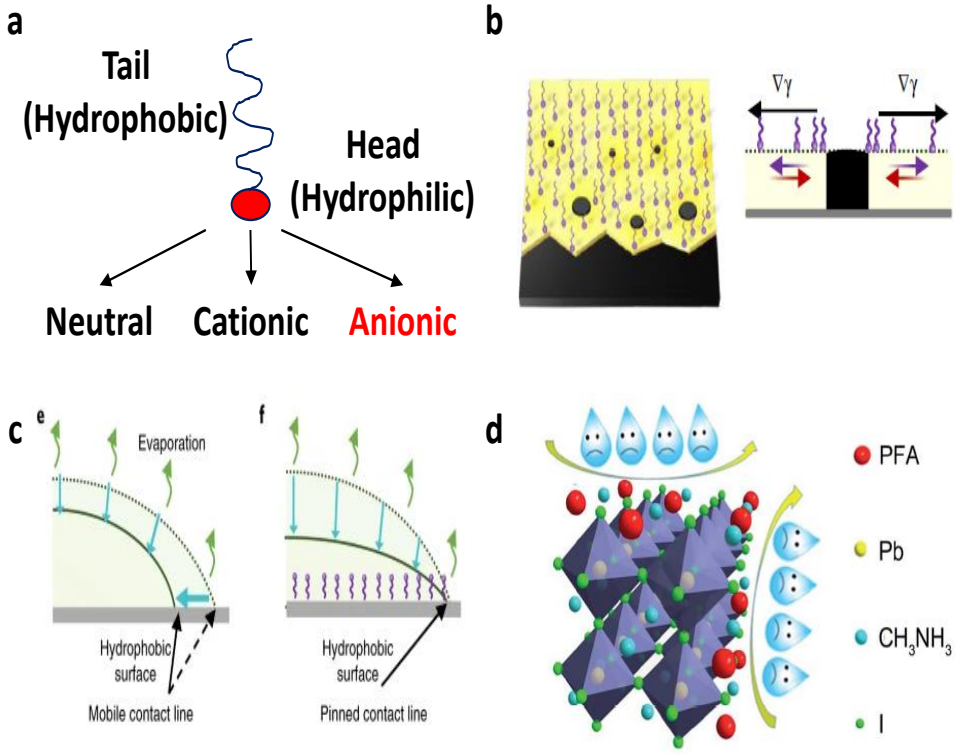

Figure 1.4. a. Schematic illustration of surfactants. b. Schematic image for the solution flow dynamics suppressed by surfactants. c. Schematic illustration for the surfactant pinning effect on hydrophobic surface.[47] d. Schematic image of preventing water and oxygen penetration by surfactants.[48]

Chapter 2. Experimental

2.1. Fabrication of Perovskite Solar Cells

For the perovskite and PCBM precursor, several materials were required such as lead iodide (PbI_2), potassium perfluorobutane sulfonate (PFC), methylammonium iodide (MAI), and [6,6]−phenyl−C_{60}−butyric acid methyl ester (PCBM). Additionally, dimethyl formamide (DMF), dimethyl sulfoxide (DMSO), and chlorobenzene (CB) were used as solvents.

For the NiO_x precursor, several materials were required such as nickel (II) nitrate hexahydrate and copper (II) nitrate trihydrate. Additionally, ethylene glycol and ethylenediamine were used as solvents.

For washing the ITO glasses, they were sonicated with deionized (DI) water, acetone, and isopropanol (IPA) for 15 minutes, respectively. After the washing, they were treated with UV/O_3 to make the hydrophilic surface.

Fabrication of NiO_x layer: the ethylene glycol solution containing 0.4 M nickel (II) nitrate hexahydrate and 0.02 M copper (II) nitrate trihydrate with 1 molar equivalent of ethylenediamine was mixed at 60 ℃ for 12 h. In this stage, the copper−doped nickel exhibited excellent electrical properties.[56] The NiO_x precursor was spin−coated on the UV−treated ITO glass at 4000 rpm for 90 s. Then, the substrates were annealed at 150 ℃ for 30 min and 400 ℃ for 30 min, respectively. After the cooling, they were put in a glove box (Figure 2.1a).

Fabrication of perovskite layer: the 1.53 M perovskite precursor contained PbI_2:MAI=1.045 in DMF:DMSO=8:1 (v/v) was mixed at 60 ℃ for 12 h. For the precursor containing surfactants, 0.01 solution wt% of PFC in DMF:DMSO=8:1 (v/v) was added in this step. In this step, the high concentration of PFC surfactants interfered with the formation of the perovskite films (Figure 2.2). Then it was spin−coated on the NiO_x coated ITO glasses at 4000 rpm for 50 s. At this stage, 0.5 mL of CB was rapidly dropped by spin−casting at 41 s. And then, the ITO glasses were annealed at 100 ℃ for 15 min (Figure 2.1b).

Fabrication of PCBM layer and metal electrode: the 20 mg/mL PCBM in chlorobenzene was mixed at 60 ℃ for 12 h. Then it was spin coated on the perovskite layer at 1000 rpm for 60 s and at 2000 rpm

for 1 s, respectively. Finally, 7 nm BCP and 100 nm Ag was deposited by using thermal evaporator (Figure 2.1c). All the thermal evaporation processes were conducted at the high vacuum condition, 5 x 10^{-6} Torr.

2.2. Measurements

The XRD patterns of perovskite films were obtained using a D8-Advance a1 system (BRUKER MILLER Co.). The XPS data were obtained with a SIGMA PROBE (ThermoFisher Scientific, U.K). The SEM images were recorded using a JSM-7800F Prime (JEOL Ltd, Japan). The AFM images were obtained using a NX-10 (Park Systems). The PL and TRPL data were obtained using FlouTime 300 (PicoQuant). The UV-vis spectra were recorded using a V-770 spectrophotometer (JASCO).

The characteristics of perovskite solar cells were measured using a Keithely 2400 sourcemeter under simulated AM 1.5 G irradiation produced by 300 W Xenon lamp solar simulator. The voltage range was -0.5 V to 1.2 V with a step voltage of 0.02 V/s and delay time of 100 ms, the area of solar cells was measured to be about 1.2 x 10^{-5} m^2. At this stage, the delay time played an important role in controlling the hysteresis of the perovskite solar cells. The perovskite solar cells with 100 ms delay time showed one quarter to a fifth of the HI compared to the 0 ms delay time measurements (Figure 2.3 and Table 2.1). CV measurements were carried out in the dark at the range of -0.5 V to 0.5 V and a constant frequency of 10 kHz and an AC amplitude of 20 mA.

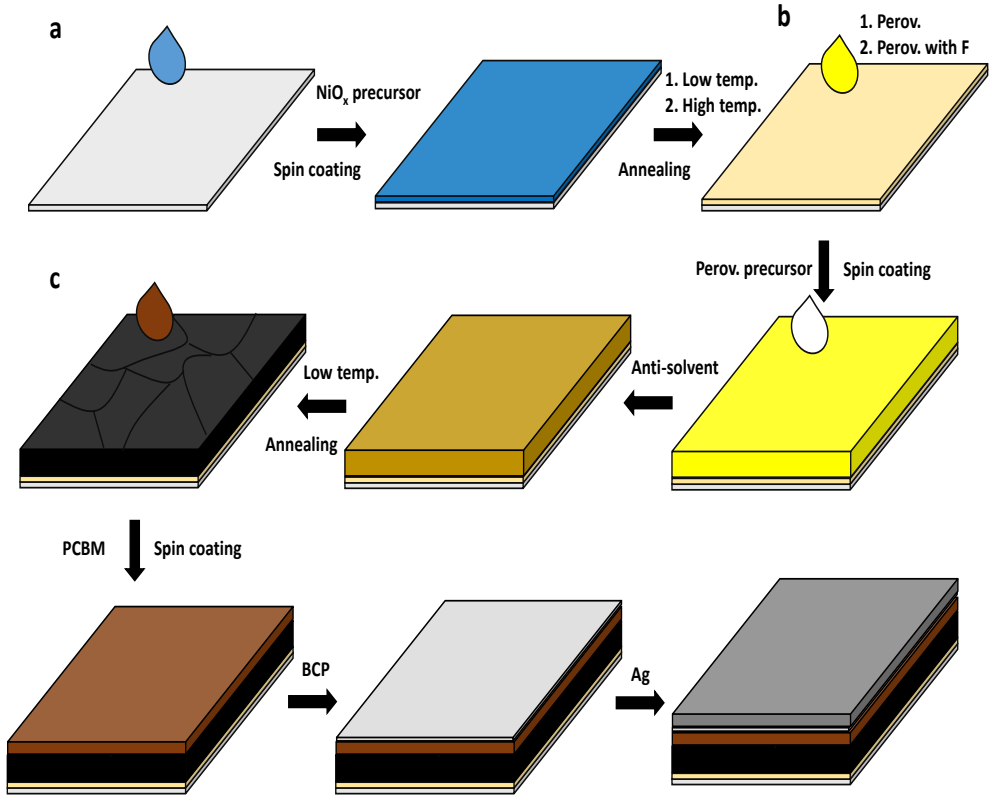

Figure 2.1. Schematic image of the fabrication process of perovskite solar cells. a. Fabrication of NiO_x hole transport layer. b. Fabrication of perovskite layer c. Fabrication of PCBM layer and metal electrode.

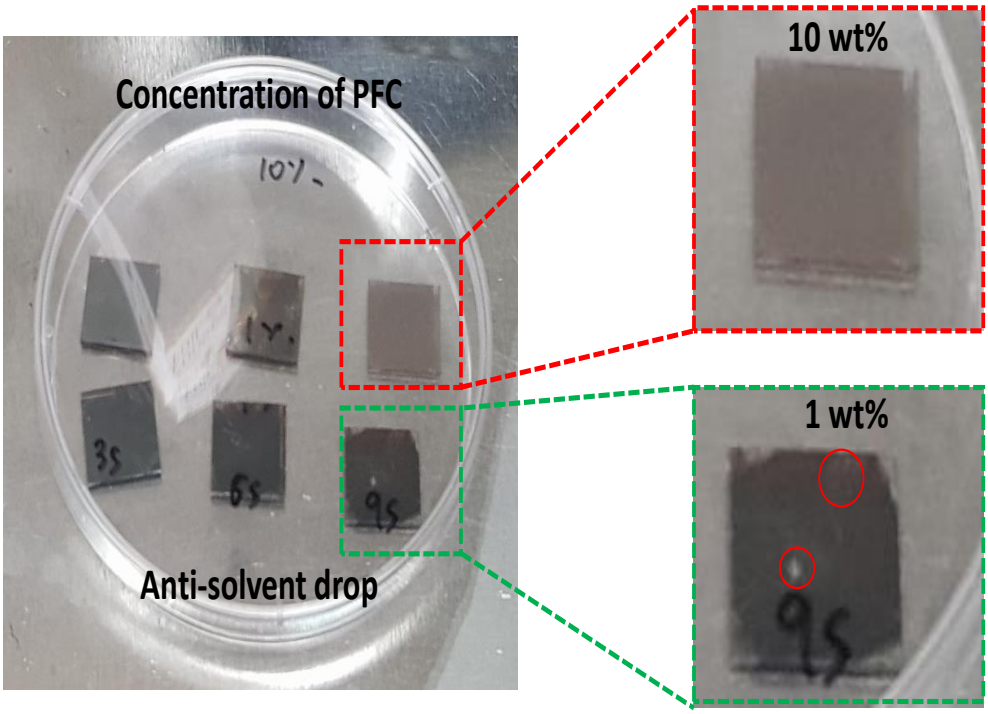

Figure 2.2. Images of the perovskite films with high PFC surfactant concentrations. The red circles indicate cracks in perovskite films.

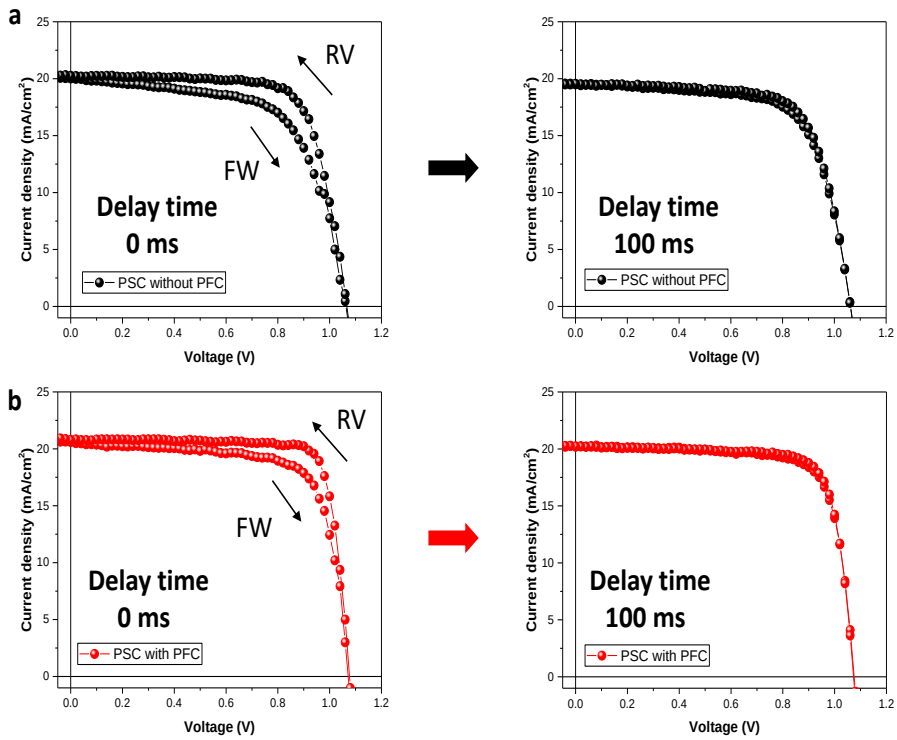

Figure 2.3. Current density−voltage($J-V$) curves of the perovskite solar cells with different delay time(0 ms and 100 ms). a. For perovskite solar cell without PFC surfactants. b. For perovskite solar cell with PFC surfactants.

Table 2.1. Performance and hysteresis index(HI) of the perovskite solar cells with different delay times.

Condition	Scan direction	J_{sc} (mA cm^{-2})	V_{oc} (V)	FF (%)	PCE (%)	HI (%)
PSC without PFC 0 ms delay time	Forward (FW)	20.0	1.06	63.9	13.6	14.5
	Reverse (RV)	20.3	1.07	73.6	15.9	
PSC with PFC 100 ms delay time	Forward (FW)	19.5	1.06	68.6	14.2	3.4
	Reverse (RV)	19.6	1.06	71.0	14.7	
PSC without PFC 0 ms delay time	Forward (FW)	20.6	1.07	73.0	16.1	12.5
	Reverse (RV)	20.8	1.08	82.2	18.4	
PSC with PFC 100 ms delay time	Forward (FW)	20.2	1.08	76.3	16.6	2.4
	Reverse (RV)	20.2	1.07	78.1	17.0	

Chapter 3. Results and Discussions

3.1. Characterization of Perovskite Films

The X-ray diffraction (XRD) peaks were well matched with the previously reported XRD peak of the solution processed $MAPbI_3$ perovskite[57], which indicated that our perovskite films were well formed during optimized spin coating conditions. However, the XRD peaks for perovskite and perovskite with PFC surfactants showed a significant difference between PbI_2[58] (red line box) and MAI-DMF-PbI_2 intermediate[59] (green line box) peaks (Figure 3.1c). The lower peak of PbI_2 could be concluded that the addition of PFC decreased surface tension of precursor and increased affinity with the substrate during the crystallization processes, as results, over-crystallization of PbI_2 was inhibited.[60] Unusually, the MAI-DMF-PbI_2 intermediate peak was clearly observed in our perovskite film, which might be caused by using the high concentration of the perovskite precursor in order to increase the thickness of the perovskite layer. Fortunately, the use of PFC surfactants suppressed the formation of the perovskite intermediates. This results could be thought that the addition of PFC facilitated the extraction of solvents such as DMF and DMSO, resulting the transition of the intermediate phase to the cubic phase was promoted. The X-ray photoelectron spectroscopy (XPS) measurements revealed that a shift of about 0.1 eV for the Pb 4f peak was observed when the PFC was added. This result was quite different from the amine based PFC surfactants. The amine-based PFC acted weak Lewis base, lowering the surrounding Pb bonding peaks.[48] Here in, the anion-based PFC surfactants might be thought to have the different mechanism, the direct electron donation. Additionally, the similarity to the shift when Pb was electron-donated[59] indicated that the uncoordinated Pb was passivated by SO_3^- of PFC (Figure 3.1d).

The scanning electron microscope (SEM) measurement showed that the addition of PFC had no effect on the grain size. Each grain

size distributions showed the similar trends, indicating that PFC did not participate in perovskite crystal growth in the planar direction (Figure 3.2a, b). Interestingly, in the cross-section SEM results, the pinhole defects were not observed between the NiO_x layers and perovskite with PFC layer (Figure 3.2c, d). This result indicated that precursor wetting process occurs well on the hydrophobic NiOx surface. The formation of pinhole defect was minimized by addition of PFC, and then, the vertical growth is facilitated through suppression of over-crystallization at the interfaces. This phenomenon was expected to improve the J_{sc} of perovskite solar cells.

The photoluminescence (PL) measurement showed high PL values when the PFC was added to perovskite. This showed that the anionic surfactant passivated defects in the grain boundary and surface, which act as non-radiative recombination sites. Interestingly, after deposition of the PCBM layers on the perovskite layers, PL showed that the perovskite with PFC exhibited a large quenching effect, indicating good charge transport from perovskite to PCBM layer(Figure 3.3a).

The time-resolved photoluminescence (TRPL) measurements confirmed charge transport from perovskite to PCBM layer. The TRPL showed that charge carrier lifetime of perovskite with PFC was significantly reduced. This results were similar to the previous PL results, meaning that the presence of PFC was related to charge transfer from perovskite to the PCBM layer (Figure 3.3b). One possible mechanism was the formation of a smooth perovskite surface. However, the AFM measurement indicated that the surface roughness of perovskite layers would not rely on the existence of PFC. The other adapted mechanism might be the formation of many PCBM crystal domains on perovskite with PFC layer. The addition of PFC made perovskite surface hydrophobic, which enhanced the crystallinity of PCBM, resulting in improved electron charge transport (Figure 3.3c). Another possible mechanism might be considered that the PFC, located between the interfaces, led to dipole reduced trapping effects, allowing the trapped photo-generated charge to be easily extracted.[61]

3.2. Device Performance and Characterization

The PFC, referred to CF−SO_3, exhibited better performance than amine−PFC, referred to CF−Am (Figure 3.4, Table 3.2). It might be considered that the better improvement of performances with the PFC was based on the higher electron donating effects and strong dipole strength of the anionic surfactant heads. The concentrations of PFC directly affected the growth of perovskite films, meaning that low concentrations of PFC was required (Figure 2.2). Comparing the efficiencies of below 0.1 wt% PFC concentration, the 0.01 wt% of PFC showed the highest efficiency, and then increasing concentration of the PFC led to a decrease in efficiencies (Figure 3.5, Table 3.3). These results indicated that when the above 0.01 wt% of PFC was added, the perfluorocarbon chains of PFC could act as insulators or modify the substrates too hydrophobic.

The perovskite solar cells optimized with PFC showed a PCE of 17.21 %, J_{sc} of 21.59 mA/cm^2, V_{oc} of 1.035 V, and *FF* of 77.08%, with almost negligible hysteresis, while the perovskite only device exhibited a PCE of 14.9 %, J_{sc} of 19.93 mA/cm^2, V_{oc} of 1.003 V, and *FF* of 74.6% (Figure 3.6a). The statistical analysis on J_{sc}, V_{oc}, *FF*, and PCE for the 25 devices revealed that the addition of PFC dramatically improves the performance of perovskite solar cells (Figure 3.6b, Table 3.4). The UV−vis data showed a slight increase in the optical band gap[62] of perovskite with PFC due to the shallow trap filling (Figure 3.6c). The CV data showed that the perovskite solar cell with PFC had a higher flat band gap, confirming that the passivation was performed by anionic surfactant (Figure 3.6d). Both data indicated that the perovskite with PFC devices had a large V_{oc} due to the passivation effect.

3.3. Stability Test of the Devices

The stability of perovskite solar cells was mainly determined by the decomposition rate of perovskite. The chemical reactions of perovskite were accelerated by air[63.64], light[65,66], and

temperature[67,68]. The main step was reaction with O_2 and H_2O by exposure to air. The chemical reaction formula was as follows[63],

$$CH_3NH_3PbI_3 \overset{H_2O}{\longleftrightarrow} CH_3NH_3I(aq) + PbI_2(s)$$
$$CH_3NH_3I(aq) \leftrightarrow CH_3NH_2(aq) + \mathrm{HI}(aq)$$
$$4HI(aq) + O_2 \leftrightarrow 2I_2(s) + 2H_2O$$
$$2\mathrm{HI(aq)} \overset{hv}{\leftrightarrow} H_2 \uparrow + I_2(s)$$

I_2, PbI_2, etc. were precipitated during the reactions with the largest proportion of PbI_2.[69] Therefore, preventing air injection to perovskite layer was one of the most reasonable ways to increase stability of perovskite solar cells. In this regard, the perovskite solar cell with PFC surfactant was expected to have the hydrophobic molecular barriers modified by perfluorocarbon chains.

The stability tests were conducted with devices fabricated under the same conditions at a temperature of 20 ºC ± 2 ºC and a relative humidity (RH) of 60 ± 5%. After 7 days, yellow-colored haze was observed on the perovskite only film, which might be due to PbI_2.[57.70.71] In the case of perovskite with PFC film, the less haze was observed on surface, which might be due to the hydrophobic chain of PFC acting as molecular barriers of H_2O and O_2 (Figure 3.7a).[48] Additionally, a direct drop method was used to measure the direct resistance to H_2O. As a result, the perovskite layer with PFC film was decomposed slowly compared with the perovskite only film (Figure 3.7b).

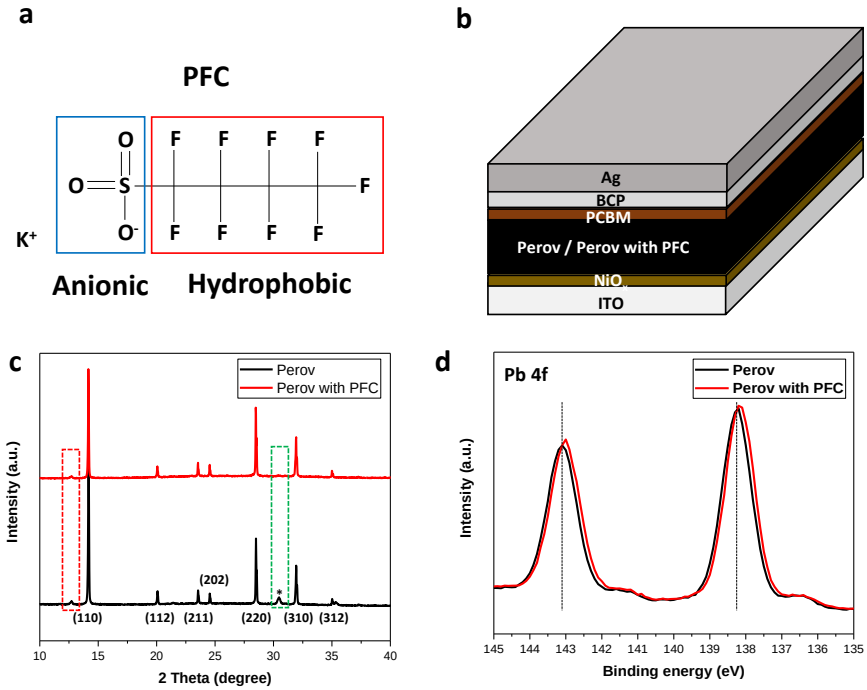

Figure 3.1. a. Molecular structure of PFC surfactant. b. Device structures of fabricated perovskite solar cells. c. XRD patterns of the perovskite and perovskite with PFC film. The red box indicates PbI_2 peak and the green box indicates MAI–DMF–DMSO intermediate peak. d. XPS spectra of the perovskite films. The dot lines, located at 138.2 eV and 143 eV, respectively, mean two maximum intensity peaks of perovskite.

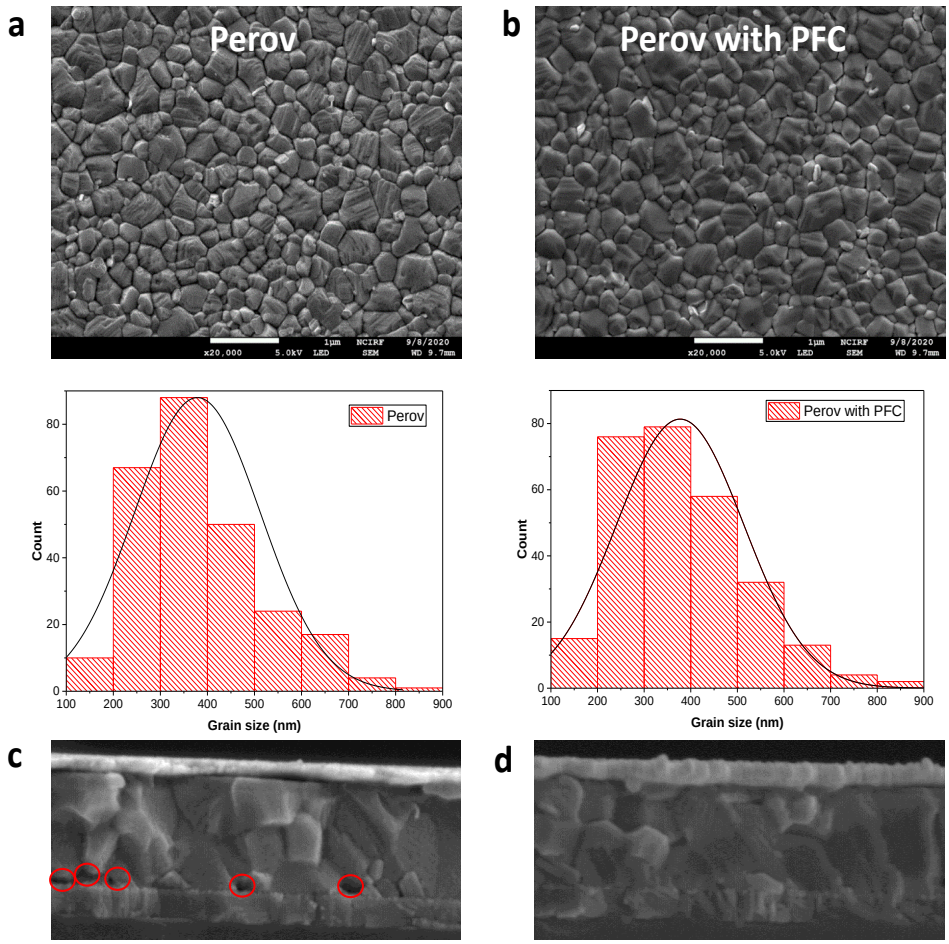

Figure 3.2. (a and b) SEM and grain size observations of the perovskite films. (c and d) Cross-sectional SEM image of the perovskite films. The red circles indicate pinholes in perovskite films.

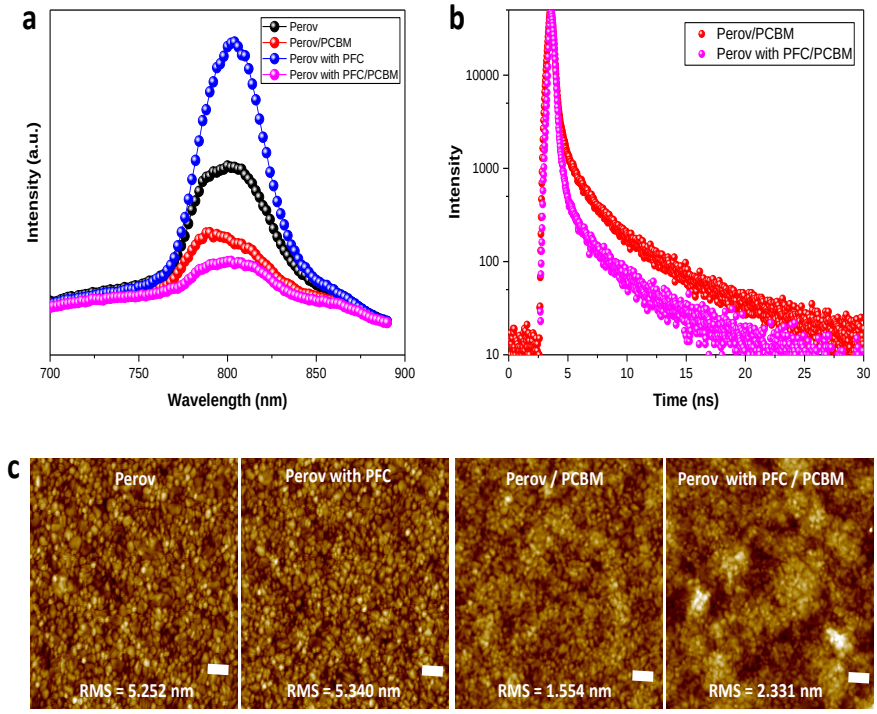

Figure 3.3. a. Steady PL of the perovskite films and with PCBM layer. b. Time-resolved PL of the perovskite films with PCBM layer. c. AFM images of the perovskite films and with PCBM layer.

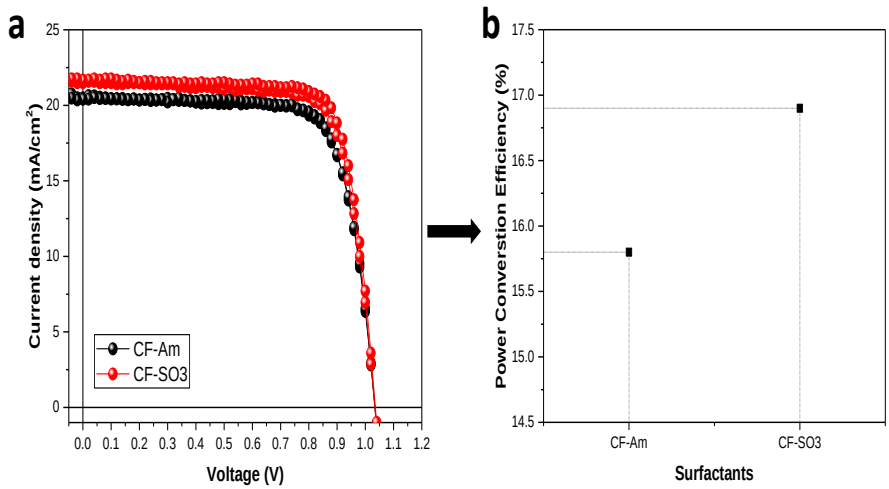

Figure 3.4. a. Current density−voltage curves in both reverse and forward directions of perovskite solar cells with different surfactants. b. Power conversion efficiency and type of surfactants plot of the perovskite solar cells.

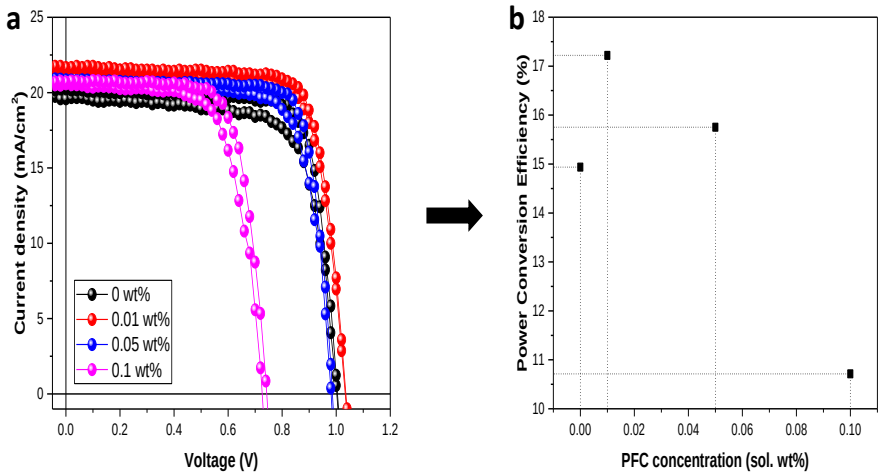

Figure 3.5. a. Current density−voltage curves in both reverse and forward directions of perovskite solar cells with various PFC surfactant concentrations. b. Power conversion efficiency and PFC concentrations plot of the perovskite solar cells.

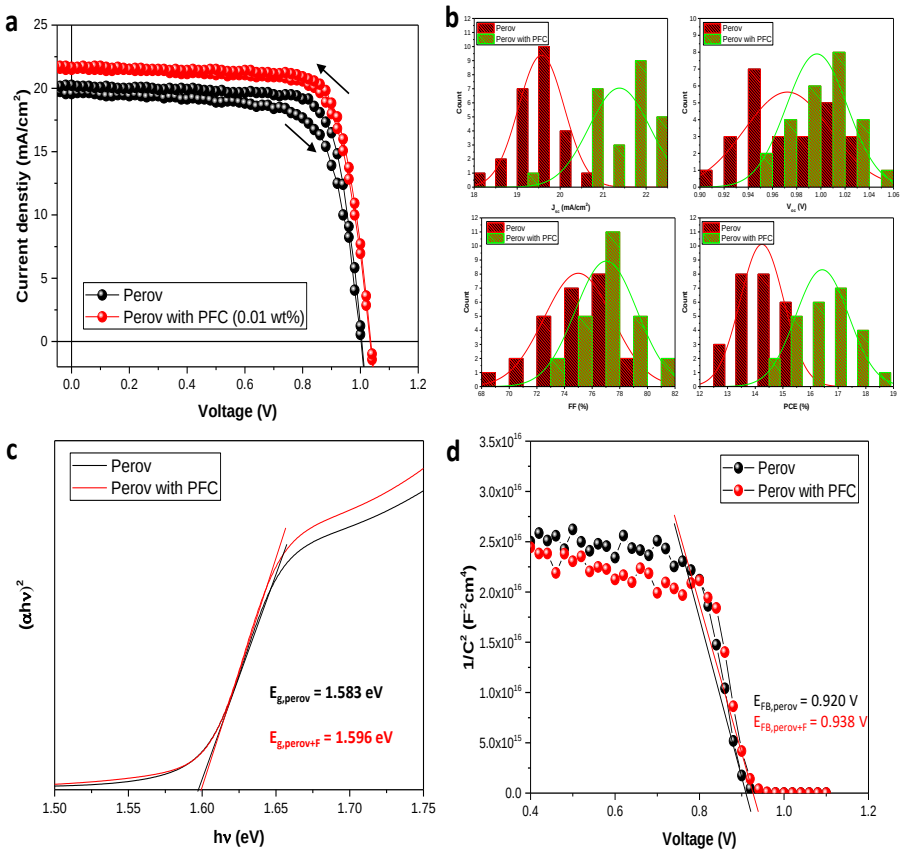

Figure 3.6. a. Current density−voltage curves in both reverse and forward directions of the perovskite solar cells. b. Distribution of J_{sc}, V_{oc}, *FF*, and PCE of the perovskite solar cells. c. Optical band gap energy determination of the perovskite films. d. *Mott−Schottky* plot for the perovskite solar cells.

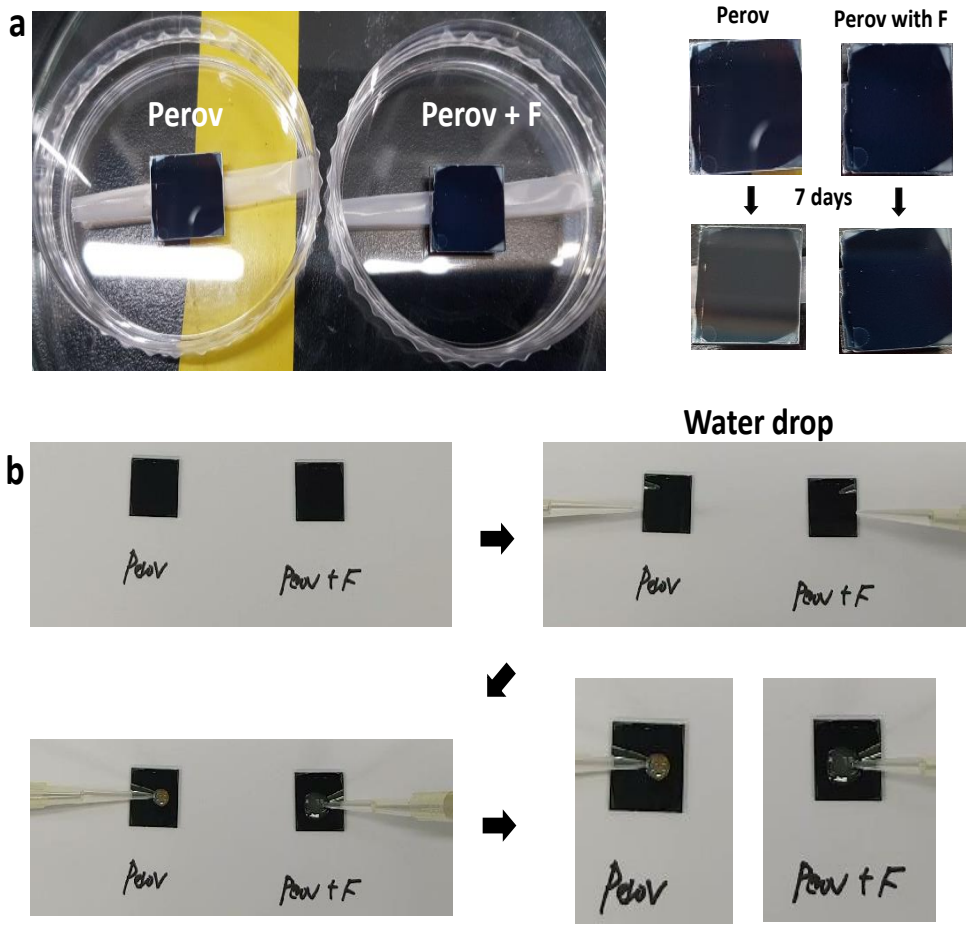

Figure 3.7. a. Images of the perovskite films and exposed to atmosphere after 7 days. b. Images of the perovskite films directly exposed to DI water. The Perov and Perov+F indicates that perovskite film without PFC and perovskite film with PFC, respectively.

Table 3.1. Grain size distribution of the perovskite films.

Condition	Counts	Mean	SD	Min.	Median	Max.
Perovskite film without PFC	261	378.74	134.07	164.10	353.85	830.77
Perovskite film with PFC	279	377.23	136.83	138.46	353.85	876.92

Table 3.2. Performance of perovskite solar cells with different surfactants.

Condition	J_{sc} (mA cm^{-2})	V_{oc} (V)	FF (%)	PCE (%)
CF-Am	20.5	1.03	74.8	15.8
CF-SO_3	21.5	1.03	76.3	16.9

Table 3.3. Performance of perovskite solar cells with different PFC surfactant concentrations.

Condition	J_{sc} (mA cm^{-2})	V_{oc} (V)	FF (%)	PCE (%)
0 wt%	19.9	1.003	74.6	14.9
0.01 wt%	21.6	1.035	77.0	17.2
0.05 wt%	22.9	0.889	74.7	15.2
0.1 wt%	20.7	0.743	72.8	11.2

Table 3.4. Average photovoltaic parameters of the optimized perovskite devices with standard deviations.

Condition	J_{sc} (mA cm^{-2})	V_{oc} (V)	FF (%)	PCE (%)
PSC without PFC	19.56 ± 0.53	0.97 ± 0.04	74.99 ± 2.48	14.24 ± 0.79
PSC with PFC	21.38 ± 0.71	1.00 ± 0.25	77.01 ± 2.24	16.42 ± 0.96

Chapter 4. Conclusion

The addition of PFC to perovskite improved the crystallinity of perovskite and suppressed the over-crystallization of PbI_2. It is thought that the addition of surfactant improved the crystallinity of perovskite film by the reduction of surface tension and good affinity with the substrate. It is considered that the addition of PFC suppresses the formation of pinhole defect and facilitates the charge transport to PCBM. The V_{oc} was increased by passivation of the uncoordinated Pb defects, confirmed through XPS, PL, UV-vis, and CV measurements. The optimized reliable perovskite solar cell functionalized with PFC showed a PCE of 17.21 %, J_{sc} of 21.59 mA/cm^2, V_{oc} of 1.035 V, and *FF* of 77.08%, with almost negligible hysteresis, exhibiting the high stability against O_2 and H_2O. Our results demonstrate that anionic surfactant additive can be used to fabricate high-performance and high-stability perovskite solar cells, and it is expected that the developed methodology can be applied not only to solar cells, but also to other optoelectronic devices including sensors.

References

[1] D. E. Carlson et al. “Amorphous silicon solar cell” *Appl. Phys. Lett.* 1976; 28:671.

[2] A. W. Blakers et al. “22.8% efficient silicon solar cell” *Appl. Phys. Lett.* 1989; 55:1363.

[3] A. Wang et al. “24% efficient silicon solar cells” *Appl. Phys. Lett.* 1990; 57:602.

[4] K, Yoshikawa et al. “Silicon heterojunction solar cell with interdigitated back contacts for a photoconversion efficiency over 26%” *Nat. Energy,* 2017; 2:17032.

[5] H. Y. Chen et al. “Polymer solar cells with enhanced open−circuit voltage and efficiency” *Nat. Photonics,* 2009; 3:649.

[6] G. Li et al. “Efficient inverted polymer solar cells” *Appl. Phys. Lett.* 2006; 88:253503.

[7] Z. He et al. “Single−junction polymer solar cells with high efficiency and photovoltage” *Nat. Photonics*, 2015; 9:174.

[8] Q. L. Song et al. “Small−molecule organic solar cells with improved stability” *Chem. Phys. Lett,* 2005; 416:42−46.

[9] Y. Huo et al. “Nonfullerene All−Small−Molecule Organic Solar Cells” *ACS Energy Lett*. 2019; 4:1241−1250.

[10] K. Gao et al. “Over 12% Efficiency Nonfullerene All−Small−Molecule Organic Solar Cells with Sequentially Evolved Multilength Scale Morphologies” *Adv. Mater.* 2019; 31:1807842.

[11] S. Liu et al. “High−efficiency organic solar cells with low non−radiative recombination loss and low energetic disorder” *Nat. Photonics,* 2020; 14:300–305.

[12] H. Zhou et al. “Interface engineering of highly efficient perovskite solar cells” *Science,* 2014; 345:6196.

[13] M. T. Horantner et al. “The Potential of Multijunction Perovskite Solar Cells” *ACS Energy Lett.* 2017; 2:2506−2513.

[14] N. Ito et al. “Mixed Sn–Ge Perovskite for Enhanced Perovskite Solar Cell Performance in Air” *J. Phys. Chem. Lett.* 2018; 9:1682−1688.

[15] M. Jeong et al. “Stable perovskite solar cells with efficiency

exceeding 24.8% and 0.3−V voltage loss" *Science*, 2020; 369:1615−1620.
[16] A. R. Chakhmouradian et al. "Celebrating 175 Years of Perovskite Research: A Tribute to Roger H. Mitchell" *Phys. Chem. Miner.* 2014; 41:387−391.
[17] Y. Yuan et al. "Arising Applications of Ferroelectric Materials in Photovoltaic Devices" *J. Mater. Chem. A* 2014; 2:6027−6041.
[18] H. L. Wells et al. "U¨ber die Ca¨sium− und Kalium−Bleihalogenide" *Zeitschrift fu¨r anorganische Chemie* 1893; 3:195−210.
[19] D. Weber et al. "$CH_3NH_3SnBr_xI_{3-x}$ (x = 0−3), ein Sn(II)−System mit kubischer Perowskitstruktur/$CH_3NH_3SnBr_xI_{3-x}$(x = 0−3), a Sn(II)−System with Cubic Perovskite Structure" *Z. Naturforsch., B: J. Chem. Sci.* 1978; 33:862−865.
[20] T. B. Song et al. "Performance Enhancement of Lead−Free Tin−Based Perovskite Solar Cells with Reducing Atmosphere−Assisted Dispersible Additive" *ACS Energy Lett.* 2017; 2:897−903.
[21] J. Li et al. "Enhanced Performance of Sn−Based Perovskite Solar Cells by Two−Dimensional Perovskite Doping" *ACS Sustainable Chem. Eng.* 2020; 8:8624−8628.
[22] T. B. Song et al. "Importance of Reducing Vapor Atmosphere in the Fabrication of Tin−Based Perovskite Solar Cells" *J. Am. Chem. Soc.* 2017; 139:836−842.
[23] S. Shao et al. "Highly Reproducible Sn−Based Hybrid Perovskite Solar Cells with 9% Efficiency" *Adv. Energy Mater.* 2018; 8: 1702019.
[24] M. A. Green et al. "The Emergence of Perovskite Solar Cells" *Nat. Photonics*, 2014; 8:506−514.
[25] D. W. deQuilettes et al. "Impact of Microstructure on Local Carrier Lifetime in Perovskite Solar Cells" *Science,* 2015; 348:683−686.
[26] Y. Zhao et al. "Solid−State Mesostructured Perovskite $CH_3NH_3PbI_3$ Solar Cells: Charge Transport, Recombination, and Diffusion Length" *J. Phys. Chem. Lett.* 2014; 5: 490−494.
[27] W. E. I. Sha et al. "The efficiency limit of $CH_3NH_3PbI_3$ perovskite

solar cells" *Appl. Phys. Lett.* 2015; 106:221104.
[28] D. Yang et al. "High efficiency planar-type perovskite solar cells with negligible hysteresis using EDTA-complexed SnO_2" *Nat. Commun.* 2018; 9:3239.
[29] I. Chung et al. "All-solid-state dye-sensitized solar cells with high efficiency" *Nature* 2012; 485:486-489.
[30] Q. Jiang et al. "Surface passivation of perovskite film for efficient solar cells" *Nat. Photonics* 2019; 13:460-466.
[31] M. A. Green et al. "Solar cell efficiency tables (Version 55)" *Prog. Photovoltaics,* 2020; 28: 3.
[32] P. Singh et al. "Temperature dependence of *I–V* characteristics and performance parameters of silicon solar cell" *Solar Energy Materials & Solar Cells*, 2008; 92:1611–1616.
[33] C. Li et al. "Iodine Migration and Its Effect on Hysteresis in Perovskite Solar Cells" *Adv. Mater.* 2016, 28;2446-2454.
[34] H. S. Kim et al. "Control of *I–V* Hysteresis in $CH_3NH_3PbI_3$ Perovskite Solar Cell" *J. Phys. Chem. Lett.* 2015; 6:4633-4639.
[35] S. N. Habisreutinger et al. "Hysteresis Index: A Figure without Merit for Quantifying Hysteresis in Perovskite Solar Cells" *ACS Energy Lett.* 2018; 3:2472-2476.
[36] G. Wang et al. "Efficient perovskite solar cell fabricated in ambient air using one-step spin-coating" *RSC Adv.* 2016; 6:43299.
[37] B. Cai et al. "Solvent engineering of spin-coating solutions for planar-structured high-efficiency perovskite solar cells" *Chinese Journal of Catalysis,* 2015; 36:1183–1190.
[38] X. Liu et al. "Boosting the efficiency of carbon-based planar CsPbBr3 perovskite solar cells by a modified multistep spin-coating technique and interface engineering" *Nano Energy*, 2019; 56:184–195.
[39] N. J. Jeon et al. "Solvent engineering for high-performance inorganic–organic hybrid perovskite solar cells" *Nat. Mater.* 2014; 13:897.
[40] C. H. Chiang et al. "Planar heterojunction perovskite/$PC_{71}BM$ solar cells with enhanced open-circuit voltage via a (2/1)-step spin-coating process" *J. Mater. Chem. A,* 2014; 2:15897.

[41] Y. Yu et al. “Ultrasmooth Perovskite Film via Mixed Anti-Solvent Strategy with Improved Efficiency” *ACS Appl. Mater. Interfaces,* 2017; 9:3667-3676.
[42] M. Li et al. “Enhanced Efficiency and Stability of Perovskite Solar Cells via Anti-Solvent Treatment in Two-Step Deposition Method” *ACS Appl. Mater. Interfaces*, 2017; 9:7224-7231.
[43] W. Li et al. “Enhanced UV-light stability of planar heterojunction perovskite solar cells with caesium bromide interface modification” *Energy Environ. Sci.* 2016; 9:490-498.
[44] H. Li et al. “Interface Modification for Enhanced Efficiency and Stability Perovskite Solar Cells” *J. Phys. Chem. C,* 2020; 124: 12948-12955.
[45]P. W. Liang et al. “Additive Enhanced Crystallization of Solution-Processed Perovskite for Highly Effi cient Planar-Heterojunction Solar Cells” *Adv. Mater.* 2014; 26:3748–3754.
[46] X. Gong et al. “Controllable Perovskite Crystallization by Water Additive for High-Performance Solar Cells” *Adv. Funct. Mater.* 2015; 25:6671–6678.
[47] Y. Deng et al. “Surfactant-controlled ink drying enables high-speed deposition of perovskite films for efficient photovoltaic modules” *Nat. Energy* 2018; 3:560-566.
[48] P. Guo et al. “Surface & grain boundary co-passivation by fluorocarbon based bifunctional molecules for perovskite solar cells with efficiency over 21%” *J. Mater. Chem. A* 2019; 7:2497.
[49] N. Kuramoto et al. “Micellar chemical polymerization of aniline” *Synthetic Metals,* 1995; 68:191-194.
[50] D. Han et al. “Reversed micelle polymerization: a new route for the synthesis of DBSA–polyaniline nanoparticles” *Colloids and Surfaces A: Physicochem. Eng. Aspects*, 2005; 259:179–187.
[51] K. Kataoka et al. “Block copolymer micelles for drug delivery: Design, characterization and biological significance” *Advanced Drug Delivery Reviews*, 2012; 64:37–48.
[52] K. Kataoka et al. “Block copolymer micelles as vehicles for drug delivery” *Journal of Controlled Release,* 1993; 24:119-132.
[53] Z. Li et al. “A nonionic surfactant simultaneously enhancing

wetting property and electrical conductivity of PEDOT:PSS for vacuum–free organic solar cells" *Solar Energy Materials & Solar Cells*, 2015; 137:311–318.
[54] X. Li et al. "Non–ionic surfactant–novel agents to realize high efficiency non–fullerene opaque and semitransparent organic solar cells with Enhanced Stability" *Organic Electronics,* 2018; 62:195–202.
[55] A. K. Jena et al. "Halide Perovskite Photovoltaics: Background, Status, and Future Prospects" *Chem. Rev.* 2019; 119:3036–3103.
[56] K. H. Kim et al. "Effects of Cu doping on nickel oxide thin film prepared by sol–gel solution process" *Optik* 2014; 125:2899–2901.
[57] M. Wang et al. "A comparative study of one–step and two–step approaches for $MAPbI_3$ perovskite layer and its influence on the performance of mesoscopic perovskite solar cell" *Chem. Phys. Lett.* 2018; 692:44–49.
[58] Z. Huang et al. "Highly Efficient and Stable $MAPbI_3$ Perovskite Solar Cell Induced by Regulated Nucleation and Ostwald Recrystallization" *Materials*, 2018; 11:778.
[59] X. Guo et al. "Identification and characterization of the intermediate phase in hybrid organic–inorganic MAPbI3 perovskite" *Dalton Trans.* 2016; 45:3806.
[60] T. Niu et al. "Stable High–Performance Perovskite Solar Cells via Grain Boundary Passivation" *Adv. Mater.* 2018; 30:1706576.
[61] J. H. Lee et al. "Introducing paired electric dipole layers for efficient and reproducible perovskite solar cells" *Energy Environ. Sci.* 2018; 11:1742–1751.
[62] C. Wu et al. "A study on the effects of mixed organic cations on the structure and properties in lead halide perovskites" *Phys. Chem. Chem. Phys.* 2020; 22:3105.
[63] G. Niu et al. "Review of recent progress in chemical stability of perovskite solar cells" *J. Mater. Chem. A,* 2015; 3:8970–8980.
[64] J. M. Frost et al. "Atomistic origins of high–performance in hybrid halide perovskite solar cells" *Nano Lett.*2014; 14:2584–2590.
[65] T. Leijtens et al. "Overcoming ultraviolet light instability of sensitized TiO(2) with meso–superstructured organometal tri–halide perovskite solar cells" *Nat.Commun.* 2013; 4:2885.

[66] S. Ito et al. “Effects of Surface Blocking Layer of Sb_2S_3 on Nanocrystalline TiO_2 for $CH_3NH_3PbI_3$ Perovskite Solar Cells” *J. Phys. Chem. C.* 2014; 118:16995–17000.
[67] B. Philippe et al. “Chemical and electronic structure characterization of lead halide perovskites and stability behavior under different exposures a photoelectron spectroscopy investigation” *Chem. Mater.* 2015; 27:1720–1731.
[68] B. Conings et al. “Intrinsic Thermal instability of methyl ammonium lead tri halide perovskite” *Adv. Energy Mater.* 2015; 5: 1500477.
[69] J. A. Christians et al. “Transformation of the excited state and photovoltaic efficiency of $CH_3NH_3PbI_3$ perovskite upon controlled exposure to humidified air” *J. Am. Chem. Soc.* 2015; 137:1530–1538.
[70] G. Niu et al. “Study on the stability of $CH_3NH_3PbI_3$ films and the effect of post−modification by aluminum oxide in all−solid−state hybrid solar cells” *J. Mater. Chem. A,* 2014; 2:705−710.
[71] D. Wang et al. “Stability of perovskite solar cells” *Solar Energy Materials & Solar Cells,* 2016; 147:255–275.

Abstract in Korean

용액 공정상에서 결정 성장을 제어하는 것은 고성능 고안정성 페로브스카이트 태양전지를 제조하는데 있어 가장 효과적인 방법이다. 그러나 용매의 다이나믹하고 빠른 증발은 이를 실현하는데 있어 큰 어려움이 된다. 본 연구에서는 페로브스카이트 태양전지의 성능 향상을 위해 음이온계 계면활성제를 활용하는 첨가제 공법을 개발하였다. 납 기반 페로브스카이트에 음이온계 계면 활성제를 첨가하여 효율과 안정성을 높이고자 하였다. 음이온계 계면활성제는 페로브스카이트 용액의 표면 장력을 감소시켰고, 기판과의 친화도를 높여 페로브스카이트 결정 성장을 향상시켰다. 더 나아가, 음이온은 납 결함을 패시베이션하여 납 기반 페로브스카이트 태양전지의 광학적 성능을 크게 향상시켰다. 음이온계 계면활성제를 첨가하여 제조한 페로브스카이트 태양전지는 효율 17.21%를 보였으며, 기존 태양전지 대비 크게 감소된 이력 현상을 보였다. 추가적으로 음이온계 계면활성제의 첨가는 페로브스카이트의 공기와 물에 대한 안정성을 증가시켰다. 이러한 음이온계 계면활성제를 첨가하는 방법은 페로브스카이트 태양 전지의 상용화를 위한 효과적인 방법으로 제시될 수 있다.

Acknowledgements

2017년 2월 포항공과대학교 SNDL 연구실에서의 학부생 연구 참여를 시작으로, 2021년 2월 서울대학교 OPEL 연구실에서의 석사 과정을 마무리하며 그동안 도움주신 분들께 감사 인사를 올립니다.

우선 지난 4년이라는 기간 동안 연구자로 성장하도록 지도해주신 오준학 교수님에게 감사드립니다. 매번 열정적인 지도로 이끌어 주셨으나, 저의 부족함으로 교수님의 지도를 다 따라가지 못하여 죄송스럽습니다. 사회에서도 교수님의 말씀 잊지않으며, 자랑스러운 제자로 성장할 수 있도록 노력하도록 하겠습니다. 그리고 저의 학위논문심사를 위해 바쁜 와중에도 소중한 시간 마련해주신 이종찬 교수님, 유동원 교수님 감사드립니다.

지난 연구실 생활 동안 저에게 큰 힘이 되어준 SNDL, OPEL 선배님들, 동기 및 후배들에게 감사의 말을 전합니다. 포항에서부터 저를 연구자로서 이끌어주신 이윤호 박사, 김홍기 선배님 감사합니다. 그리고 제가 힘들 때 많은 도움을 주신 박철희 박사, 송인호 박사, 안재용 선배님 감사합니다. 또한 제가 연구실 생활에 잘 적응 할 수 있게 배려해주신 권오영 박사, 이무열 박사, 이해랑 박사, 이도영, 정아영, 한명근, 한슬기 선배님 감사합니다. 지난 2년간 큰 힘이 되어준 원유상, 박종민 동기들에게 진심으로 감사합니다!

2014년 포항에서 만난 인연으로 시작하여, 지금도 좋은 친구로 지내는 14분반, 화공과 및 좋은 인연으로 맺어진 여러분들께. 덕분에 포항에서의 4년이라는 시간이 좋은 추억으로 남을 수 있었습니다. 대단히 감사합니다!

마지막으로, 저에게 매번 큰 도움이 되어준 가족들에게 감사 인사를 전합니다.